

Absolute-cross-section measurements for electron-impact ionization of triply charged inert-gas ions: Ne^{3+} , Ar^{3+} , Kr^{3+} , and Xe^{3+}

D. C. Gregory, P. F. Dittner, and D. H. Crandall

Physics Division, Oak Ridge National Laboratory, Oak Ridge, Tennessee 37830

(Received 25 August 1982)

Electron-ion crossed beams have been employed to obtain absolute cross sections for single ionization of Ne^{3+} , Ar^{3+} , Kr^{3+} , and Xe^{3+} . These data reveal a steady progression from excellent agreement with theory and semiempirical formulas for Ne^{3+} to significant departures from any simple models for Xe^{3+} . For Ar^{3+} some small departure from the models is apparent and the measurements agree with previous experimental results of Müller *et al.* For Kr^{3+} and Xe^{3+} the measured cross sections in the energy range below four threshold units exhibit complex structure and exceed estimates of direct ionization by roughly factors of 2 and 3, respectively. These features are attributed to indirect ionization processes involving excitation of inner-shell electrons, and the observed cross-section shapes imply that the excitation-autoionization features cannot be simply attributed to dipole-allowed excitation transitions. Ionization rates for Maxwellian electron-temperature distributions are calculated from the data.

I. INTRODUCTION

Electron-impact ionization is a subject of continuing interest. Ionization is one of the processes essential to understanding the behavior of laboratory and astrophysical plasmas¹ but agreement between experiment and theory is still elusive.

The usual sources of cross sections for plasma modeling are scaling laws and semiempirical formulas.² The most widely used formula is due to Lotz³ and the single parameter representation given here is both trivial to use and generally as reliable as any available prediction for light ions⁴:

$$\sigma(E) = 4.5 \times 10^{-14} \sum_j \frac{r_j}{I_j E} \ln(E/I_j), \quad (1)$$

where the cross section σ at a collision energy E (in eV) is given in cm^2 , r_j is the number of electrons in subshell j , and I_j is the ionization energy (in eV) for electrons in that subshell. The Lotz formula is based on measurements for singly charged ions and on Coulomb-Born theory for infinite Z hydrogenic ions. A number of quantal calculations for specific ions, including some of the currently studied ions, have been carried out in Coulomb-Born and distorted-wave approximations. However, all of these representations of ionization have been based on direct ejection of individual electrons from the ion.

In 1968, Bely⁵ gave specific predictions for Na-like ions which suggested that inner-shell excitation followed by autoionization would give significant enhancement of ionization cross sections and that

the importance of this process would increase significantly with ionic charge q along the isoelectronic sequence. Also in 1968, crossed-beam measurements on singly charged alkali-metal-like ions^{6,7} failed to show the predicted excitation-autoionization effect in Mg^+ but did demonstrate significant cross-section enhancement for the heavier alkali-metal-like ions. Those measurements indicated increasing importance of the indirect processes as the atomic number Z of the ion increased. Excitation-autoionization effects are characterized by sharp increases in the ionization cross section at threshold energies, a shape characteristic of excitation of ions.

Recent experiments have investigated ions of initially higher ionic charge.⁸⁻¹² Some of these experiments have studied charge-state effects along isoelectronic sequences for Li-like⁹ and Na-like¹⁰ ions and have demonstrated increasing importance of indirect effects with increasing ionic charge. One cooperative effort between experiment and theory gained considerable insight from a study of triply charged alkali-metal-like ions.¹² Indirect effects were found to dominate by roughly a factor of 10 over direct ionization. However, this work also predicted that the states responsible for the largest indirect effects in the heavy alkali-metal-like ions would become bound (nonautoionizing) for higher ionic charges. A simple increase of excitation-autoionization with increasing ionic charge should not always be anticipated.

In addition to excitation-autoionization there is some evidence for at least one other indirect process

contributing to electron-impact ionization. LaGatuta and Hahn¹³ suggested that formation of highly excited recombination resonances followed by double Auger autoionization would significantly enhance electron-impact ionization of Na-like Fe^{15+} . Henry and Msezane¹⁴ have applied this process to interpret details of the measured ionization cross section for Na-like Al^{2+} . These recombination resonances to high nl states are associated with inner electron excitations, resulting in a highly excited bound state in which a dominant decay mode is double autoionization. The resonances observed in dielectronic recombination and in bound-state excitation cross sections are similar except that in the present process a net single ionization is the end product of the original collision event. Recombination resonances occur at lower energies than the associated inner-shell excitation and can influence the measured ionization cross-section shape by extending the expected sharp excitation onset toward lower energies.

Although excitation-autoionization contributions have been predicted for Mg-like¹⁵ and for B- and Be-like ions^{16,17} and have been observed in isolated cases,¹⁸ almost all of the theoretical and experimental efforts to date have concentrated on alkali-metal-like ions (examples are Refs. 5–10 and 12–19). A previous study on a series of charge states of one element¹¹ did not reveal strong indirect effects, and studies on multiply charged light ions¹⁸ showed only weak indirect effects except in alkali-metal-like cases.

The choice of ions studied in the present experiments was influenced by a number of factors; the most obvious being ease of ion source operation. In addition these ions provide a target of intermediate complexity (neither the single outer-electron nor the closed-outer-shell structures commonly studied in the past). By studying ions of the same charge from the same column of the periodic table, systematic effects may be revealed which depend only on the inner-shell electron structure. Further, the specific cases studied here may be of direct value in plasma diagnostics since Ne and Ar have been deliberately injected as diagnostic impurities in tokamaks and Kr is to be used in the next generation tokamaks.²⁰

The present experimental results will be compared to the Lotz prediction and to quantum calculations where available. The predictions only represent direct electron removal so that indirect effects will be seen as abrupt departures from these calculations. In principle, distorted-wave with exchange (DWX) calculations by Younger²¹ should be the most reliable predictions but of these target ions, they are only available for Ne^{3+} and Ar^{3+} . The scaled Coulomb-Born formula of Golden and Sampson²²

will not be applied for comparisons here because the present cases are not within their stated range of validity ($q \geq Z/2$) and because the results are neither as trivial to obtain as the Lotz predictions nor as well founded in principle as Younger's DWX. In applying the Lotz formula to Kr^{3+} and Xe^{3+} we divide the d electron contribution by 2. This *ad hoc* modification has been suggested from experiments²³ on Zn^+ and Ga^+ and will be seen to improve high-energy agreement in the present cases for both Kr^{3+} and Xe^{3+} . It is possible that little or no single ionization is produced by the direct ejection of $4d$ electrons in Kr^{3+} and Xe^{3+} , since the resulting excited $4+$ ion may autoionize.

II. EXPERIMENTAL TECHNIQUE

The intersecting beam experimental technique has been reviewed²⁴ and a detailed description of the 90° crossed-beams approach with features common to the present study has been given.²⁵ Figure 1 is a drawing of the main interaction chamber. Since specific descriptions of the Oak Ridge National Laboratory-Penning Ion Gauge (ORNL-PIG) ion source²⁶ and the beam-interaction chamber^{8,10} have been presented previously, discussion here can be limited.

For 90° crossed beams, cross sections are determined from

$$\sigma(E) = \frac{\mathcal{R}}{I_i I_e} \frac{q e^2 v_i v_e}{(v_i^2 + v_e^2)^{1/2}} \frac{\mathcal{F}}{D}, \quad (2)$$

where $\sigma(E)$ is the absolute cross section at energy E , \mathcal{R} is the signal count rate, I_i and I_e are the ion- and electron-beam currents, respectively, q is the charge of incident ions, e is the charge on an electron, v_i and v_e are the ion and electron velocities, \mathcal{F} is the form factor describing beam overlap, and D is the

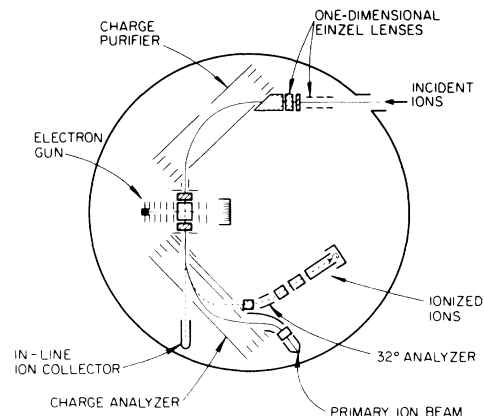


FIG. 1. Crossed-beam collision chamber viewed from above.

absolute signal detection efficiency. Each of these quantities must be carefully and independently measured in order to obtain an accurate absolute cross section. The electron beam was chopped in order to separate true signal produced in beam-beam interactions from background events. The difference in the count rates with and without electrons gives the signal rate \mathcal{R} , since the electron beam itself produced no measurable background counts in the ionization detector.

A. Ion beams

All ion beams were produced from the corresponding inert gas in the ORNL-PIG source and accelerated by 10.0 kV to produce 30.0-keV beams. An ion beam of selected m/q is obtained by the use of crossed electric and magnetic fields. This beam is transported about 2 m through two stages of collimation and differential pumping before entering the main interaction chamber shown in Fig. 1. After passing through one-dimensional Einzel lenses, the beam enters an electrostatic analyzer which eliminates any ions which have changed charge due to collisions in the beam-transport system. Lorentz deflection due to the electron gun's magnetic field is compensated by vertical deflectors before and after the interaction volume. The ion beam then enters an electrostatic analyzer which separates the $3+$ charged beam from the further ionized $4+$ ions. The $3+$ ion beam is collected in a Faraday cup, while the $4+$ ions are further deflected and focused into a channeltron for counting. Typical currents at the final ion-beam cup averaged 80 nA, with signal-to-noise ratios ranging from 1 for Ne^{3+} to 9 for Xe^{3+} .

The ion beam can be focused, deflected, and/or monitored at more than 10 points along its path. Significant time is given to optimizing beam quality with primary attention given to stable and complete overlap at the beam intersection, minimum noise in the signal channel, and maximum (near 100%) transmission of the beams from the intersection point to the proper collectors. Ion current to the apertures at the final analyzer entrance is monitored and minimized (generally required to be less than 1%) since all ions must be accounted for downstream of the interaction volume. An in-line ion collector is periodically used (with analyzer voltage off) to monitor beam transmission through the final analyzer. After the signal-channel exit of the final analyzer, all lens and deflector voltages are scanned to assure total collection of the signal ions. Transmission of signal ions is occasionally further tested by passing a $q=4+$ ion beam through the system and measuring transmission [typically 100(± 2)%] of this beam to the channeltron (operat-

ed as a Faraday cup for this test).

Metastable ions in the incident beam are possible for all four of these ions. Direct determination of metastable content of the beams was not possible in the present experiments. As a first guess, the metastable-to-ground fraction may be assumed to be statistical if the average energy of electrons in the ion source is several times the metastable-to-ground level energy difference. Such an estimate implies up to 80% metastable content in the present ion beams.

In all of the present cases, these low-lying metastable states have the same outer electron configuration as the ground state (ns^2np^3). Thus, the cross section for direct ionization of metastable ions is expected to have the same energy dependence and roughly the same magnitude as that of ground-state ions. At energies where the cross section is slowly varying (higher energies), little effect is expected in the measured cross sections due to metastables in the beam. Features that change quickly with energy, such as the initial rise in cross section near threshold or at the onset of indirect ionization (where a discontinuous increase is expected), may appear to be shifted, broadened, or perhaps even multisteped due to the metastables. Thus excitation-autoionization effects may be more difficult to analyze because of superposition of several energy-level schemes as well as the broadening of sharp features.

The electron configuration for the ground states of these ions is $ns^2np^3\ ^4S_{3/2}^o$ with the nearby metastable levels being $np^3\ ^3D^o$ and $np^3\ ^2P^o$. For Ne^{3+} these levels are 5.1 and 7.7 eV above the ground state, respectively, while for Ar^{3+} the comparable levels are at 2.6 and 4.3 eV.²⁷ No detailed information on metastable levels for Kr^{3+} is readily available. For Xe^{3+} , there are four metastable levels within 5 eV of the $5s^25p^3\ ^4S_{3/2}^o$ ground state.²⁸ It was not possible to extract the ground-state cross section or beam metastable fraction from the present data.

B. Electron beam

The electron gun used in this experiment was adapted from a design produced at Joint Institute for Laboratory Astrophysics (JILA) and described by Taylor *et al.*²⁹ The electron beam is magnetically confined. Electron energies are corrected for space-charge effects. Contributions to the collision energy due to finite ion velocity range from 0.8 eV for 30-keV Ne^{3+} ions to 0.1 eV for Xe^{3+} . Possible shifts in potential at the beam-interaction region due to the nearby deflector plates are estimated to be less than 0.1 eV, and are not corrected since the deflectors were operated at low voltage and symmetric to

minimize this effect.

The energy spread in the electron beam is important since any sharp feature in the cross section will be convoluted with the electron energy distribution. Based on the features observed in these measurements and in previous measurements under similar conditions, a 2-eV full width at half maximum (FWHM) electron-energy distribution is estimated.

C. Uncertainties

The majority of the individual measurements presented here are independently absolute. The data and corresponding statistical uncertainties at the 1 s.d. level are listed in Table I and are plotted in Figs. 2–6 when they are larger than the symbols. Additional systematic uncertainties common to all data are listed in Table II. These uncertainties are associated with quantities used in Eq. (2) to obtain the absolute cross section.

Some sets of several data points were normalized by a constant scale factor to carefully documented representative absolute calibration points. These renormalization factors changed the cross section values between 1% and 7% and they were applied to a small fraction of the data. All of the Ne^{3+} data are independently absolute while about 15% of the data for Ar^{3+} and Kr^{3+} were subjected to renormalization. For Xe^{3+} only data above 490 eV were renormalized. The deviations which are removed by renormalization are probably due to undetected variations in beam overlap or to a failure to transmit all of the signal ions to the channeltron. At the highest electron energies, background gas generation or electron-beam space charge may produce minor refocusing of the ion beam which could cause some signal ions to be lost (depending on ion beam tuning). These renormalization corrections are generally outside the reproducibility of the absolute calibration points, which are measured with beam-component transmissions and beam overlap factors carefully optimized.

Table II lists absolute uncertainties at a level judged equivalent to 90% confidence level (CL) for statistical uncertainties. The statistical uncertainty (given as $\pm 2\%$ at 90% CL for each species) is for a typical measurement at the peak cross section. The principal sources of uncertainty are believed to be measurement of the form factor and transmission of signal particles to the ionization detector. The total absolute uncertainty (quadrature combination of all uncertainties) is $\pm 7.4\%$ for each ion at the peak cross section.

Details of the form factor or beam overlap integral are discussed elsewhere.^{8,25} The electron beam is stable and reproducible in position and

shape over the lifetime of the cathode which can be years depending on vacuum integrity. Thus the form factor is most sensitive to the ion beam shape and position, and changes in ion source conditions or upstream tuning can in some cases produce a relative change in the form factor of several percent during a measurement. Of course, there are potential systematic errors in the measurement and calculation of the form factor (see Ref. 25). In principle, the present technique could be applied to obtain form factors with about $\pm 1\%$ relative uncertainty and about $\pm 2\%$ total absolute uncertainty but in practice the precise alignment and numerous repeated measurements which would be required are not considered productive. Relative variation of the form factor during a given set of measurements is well documented to be less than $\pm 2\%$ for our measurements and we estimate total absolute uncertainty to be $\pm 4\%$ for any given cross-section measurement. For the present data, beam profiles were measured every 1 to 2 h of data collection time. Form factors were obtained for selected electron energies so that values for the remaining energies were interpolated with variations being no more than 2%.

The channeltron efficiency is assumed to be 0.98 ± 0.02 for the impact of these ions at 30 keV. The few existing measurements³⁰ of the efficiency of these detectors obtain values near 100% for similar ion energies and operating conditions. Particle-counting efficiency also includes the ability of the electronics to process pulses originating in the channeltron. No change of the pulse-processing efficiency (0.98 ± 0.02) was observed during the time period of the measurements. Transmission of the ionized signal particles from the beam-interaction point to the channeltron is taken to be 100% for the present measurements as described under the “ion-beam” heading above. However, this total transmission factor cannot be as readily checked during the course of cross-section measurements as other parameters and a fairly large uncertainty ($\pm 4\%$) has therefore been allowed. The product of these factors—channeltron efficiency, pulse-processing efficiency, and signal particle transmission—constitute the efficiency factor D in Eq. (2), which has been taken to be 0.96 ± 0.05 for all measurements.

The uncertainties in electron- and ion-current measurements allow for both the uncertainty in actual measurement of the final collected current and in the transmission of the primary particles from the collision point to the current collectors.

Background modulation is always a danger in crossed-beams measurements. Careful tuning and chop frequency variations revealed no modulation problems in these measurements (except for varia-

TABLE I. Experimental electron-impact-ionization cross sections (10^{-18} cm²). Uncertainties are 1 s.d. (statistics only).

Energy (eV)	Ne ³⁺	Ar ³⁺	Kr ³⁺	Xe ³⁺
33.5				-0.27±0.33
36.0				-0.05±0.31
37.7				-0.03±0.26
39.3				0.33±0.22
40.3				0.01±0.38
41.3				2.47±0.23
42.3				3.98±0.40
43.2				9.22±0.18
44.3			0.21±0.77	11.93±0.25
45.2				15.83±0.26
46.3			-0.20±0.42	22.31±0.25
47.3				26.75±0.42
48.3			1.49±0.25	24.31±0.27
49.7				24.84±0.24
50.4			6.70±0.25	
51.2				28.29±0.29
52.3		-0.09±0.11	10.57±0.20	29.69±0.45
53.2				30.11±0.34
54.4		0.35±0.16	14.69±0.26	30.98±0.36
55.2				33.38±0.35
56.2			19.56±0.27	33.89±0.30
57.0		1.09±0.17		35.25±0.35
58.3			22.04±0.55	35.95±0.36
59.0		2.66±0.16		35.79±0.49
60.2			25.53±0.28	39.83±0.87
60.8		4.50±0.17		42.43±0.40
62.2			29.18±0.21	46.96±0.37
63.1		6.57±0.16		48.65±0.41
64.2			30.71±0.39	51.06±1.25
64.9		7.76±0.16		55.46±0.43
66.2			33.52±0.18	61.35±0.44
66.9		9.59±0.17		60.66±0.61
68.1				55.75±0.56
68.9		10.32±0.14	32.11±0.21	58.51±0.37
70.1			34.03±0.22	60.26±0.93
70.8		11.40±0.16		
71.6				68.05±0.26
72.2			33.84±0.21	
72.9		11.88±0.32		68.15±0.67
74.3		12.32±0.17	34.07±0.43	68.07±0.50
75.0				69.98±0.46
76.2		12.98±0.17	35.58±0.56	71.49±0.47
77.0				71.38±0.45
78.1			36.12±0.45	
79.0				75.94±0.33
80.1			35.63±0.26	
80.8				76.73±0.30
81.8		14.28±0.16	34.61±0.33	
83.9			35.22±0.36	80.99±0.53
86.2		15.40±0.17	35.82±0.37	86.68±0.57
86.8				83.11±0.55
88.0			36.25±0.25	
89.8			36.07±0.32	84.61±0.38

TABLE I. (Continued.)

Energy (eV)	Ne ³⁺	Ar ³⁺	Kr ³⁺	Xe ³⁺
91.0		15.92±0.17		87.05±1.09
91.9			35.23±0.26	
92.5	0.32±0.20			83.04±0.70
94.4	0.09±0.24		34.50±0.20	
95.7			35.64±0.24	87.00±0.21
96.5	0.52±0.24	16.73±0.08		
97.7			35.39±0.36	
98.5	0.69±0.20			83.50±0.69
100.0	1.33±0.20		34.58±0.37	
101.6	1.49±0.12			82.26±0.52
103.6				83.90±0.37
104.3	2.06±0.29			80.33±0.55
105.9	2.24±0.13	17.49±0.36	35.72±0.18	
107.8	2.23±0.31			78.22±0.41
110.0	2.32±0.29			
111.3	2.63±0.12			76.27±0.21
114.0	3.02±0.21			
115.8	3.49±0.11		35.62±0.26	
118.0	3.34±0.27			
120.3	3.69±0.18	17.94±0.19		71.11±0.42
121.8	4.05±0.10			
123.9	3.50±0.22			
125.5	4.21±0.11		33.92±0.19	65.98±0.37
130.7	4.36±0.22	18.02±0.13		
132.7				63.08±0.25
135.6	5.11±0.09		32.62±0.19	
140.4	4.83±0.17			57.77±0.27
145.2	5.50±0.06	17.94±0.16	31.29±0.15	59.20±0.61
155.1	5.52±0.14		30.12±0.30	53.45±0.26
157.4				54.25±0.24
165.2	5.94±0.14		28.55±0.30	
170.0	7.05±0.29	17.36±0.13		48.69±0.20
175.0	6.46±0.10		28.14±0.29	
182.0				49.13±0.21
184.7	6.78±0.07		27.86±0.25	46.92±0.30
194.4	7.16±0.07	17.40±0.12	27.92±0.24	48.31±0.37
199.2				46.02±0.21
214.2	7.45±0.08		26.95±0.10	44.85±0.29
219.0		17.28±0.08		47.64±0.33
228.8				43.79±0.31
234.1	7.76±0.06		25.95±0.18	
243.8		17.33±0.09		43.23±0.18
253.9	7.61±0.06		24.35±0.15	
268.4		16.64±0.08		40.0 ±0.11
273.6	8.03±0.08		23.34±0.15	
293.2	8.05±0.06	15.90±0.08	22.13±0.15	39.11±0.17
317.7	7.85±0.08			37.55±0.37
342.7	7.87±0.04	14.51±0.07	20.12±0.08	35.14±0.10
367.4	7.66±0.06			33.51±0.57
391.8	7.75±0.04	13.24±0.05	18.29±0.08	32.45±0.10
416.9	7.56±0.06			
440.5				29.54±0.10
441.7	7.29±0.03	12.27±0.17	17.05±0.07	
466.3	7.41±0.04			

TABLE I. (Continued.)

Energy (eV)	Ne ³⁺	Ar ³⁺	Kr ³⁺	Xe ³⁺
489.8				28.05±0.10
491.1	7.48±0.04	11.55±0.04	15.65±0.07	
492.4	6.97±0.04			
540.8		11.07±0.04		
542.3	6.90±0.04		14.89±0.23	
590.4		10.49±0.04		
591.6	6.37±0.04		13.67±0.19	25.14±0.08
640.8	6.36±0.06	9.68±0.05	12.84±0.19	
690.2	6.01±0.04	9.05±0.02	11.90±0.16	22.83±0.05
789.6	5.76±0.07	8.62±0.03	10.69±0.13	20.77±0.05
888.0		8.10±0.03		20.45±0.13
889.5	5.49±0.06		9.74±0.05	
986.8		7.58±0.01		18.29±0.06
989.0	5.49±0.02		9.07±0.05	
1188.0	4.84±0.04			
1235.0				16.66±0.06
1481.0		5.40±0.01		14.29±0.05
1486.0	4.23±0.02			

tions of a few percent occasionally observed for the highest energies) and no uncertainty is allowed for background modulation. One of the most convincing arguments against the presence of two-beam background modulation in these experiments derives from the measurements of zero cross sections below threshold. For interacting beam experiments it is convincingly asserted that the most important measurement is the one below threshold.^{31,32}

III. RESULTS AND DISCUSSION

A. Ne³⁺

Figure 2 shows the cross section versus electron energy for ionization of Ne³⁺. The data rise smoothly from the threshold for direct ionization of the outer electrons to the peak cross section of $8 \times 10^{-18} \text{ cm}^2$ at an interaction energy of about 280

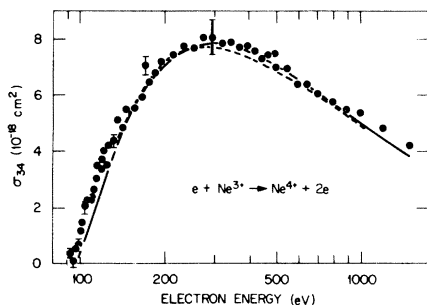


FIG. 2. Electron-impact-ionization cross section for Ne³⁺. Present data (solid points) are shown with statistical uncertainties (1 s.d.) for every measurement where they are larger than the size of the plotted points. Total absolute uncertainty at good confidence level is $\pm 7.4\%$ as shown at 295 eV. Also shown are calculations: Younger's DWX (solid line) and Lotz calculations (dashes).

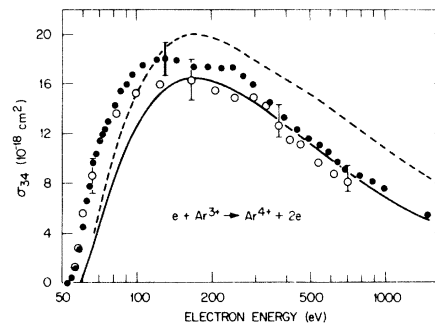


FIG. 3. Electron-impact-ionization cross section for Ar³⁺. For the present data (solid points), the statistical uncertainties are typically the size of the points. The heavy error bar at 130 eV is the total absolute uncertainty ($\pm 7.4\%$ at good confidence level). Also shown are crossed-beams measurements by Müller *et al.* (open circles), Younger's DWX theory (solid line), and Lotz calculations (dashes).

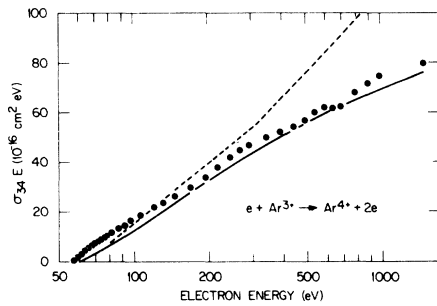


FIG. 4. Bethe plot of electron-impact ionization of Ar^{3+} . Present data (solid circles), Younger's DWX calculations (solid curve), and Lotz predictions from Eq. (1) (dashed curve) are shown.

eV. The onset of direct ionization of the $2s$ electrons at 116.3 eV does not significantly affect the total ionization. Direct ionization of the $1s$ electrons, at 971 eV, is just below the upper energy limit of the present data and has no detectable effect on total ionization. There are no unusual features in the shape of the cross section.

The rise of the Ne^{3+} cross section below 97.1 -eV ionization limit for the ^4S ground state indicates a significant metastable content in the parent ion beam. Also plotted in Fig. 2 is the Lotz calculation [see Eq. (1)] of the direct ionization cross section. Good agreement is found at all energies, even with this simple ionization model. Even though the distorted-wave calculations (including exchange) by Younger²¹ differ from the Lotz predictions by no more than 3%, Younger's cross sections are seen to be in slightly better agreement with the experimental data in the 300–600-eV range.

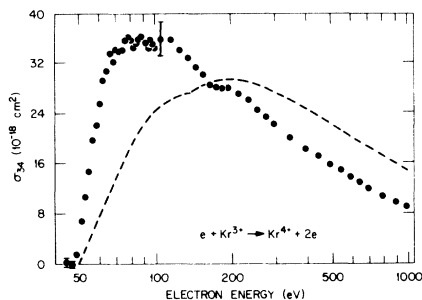


FIG. 5. Electron-impact ionization of Kr^{3+} . Present data are solid circles with statistical uncertainties (1 s.d.) shown only for the two lowest points where statistics exceed symbol size. Error bar at 105 eV is the total absolute uncertainty at good confidence level. Also shown are Lotz calculations from Eq. (1) (dashes; d -electron contribution was scaled by $\frac{1}{2}$).

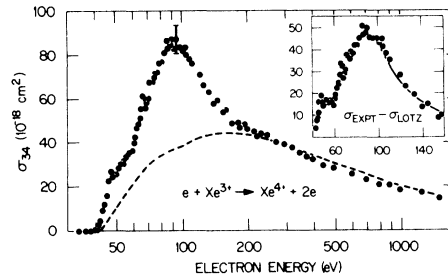


FIG. 6. Electron-impact ionization of Xe^{3+} . Statistical uncertainties (1 s.d.) are typically the size of the plotted data points. Total absolute uncertainties (good confidence level) are $\pm 7.4\%$ shown at 96 eV. Also shown is the Lotz calculation (d -electron contribution scaled by $\frac{1}{2}$). Inset: Estimated indirect contribution (experiment with Lotz subtracted) to Xe^{3+} ionization cross section. Solid line is E^{-3} falloff, characteristic of nondipole-allowed excitation to autoionizing levels.

B. Ar^{3+}

The cross section versus electron energy for ionization of Ar^{3+} is shown in Fig. 3. Direct ionization is expected to begin at 59.8 eV for the outer $3p$ electrons, and ionization of the $3s$ electrons is expected at 74 eV (no significant contribution is observed). Inner-shell electrons may be directly ionized at 308 eV ($2p$ electrons) and at 383 eV ($2s$ electrons). The

TABLE II. Uncertainties. All uncertainties are good confidence level (equivalent to 90% CL on statistical uncertainties). Uncertainties listed apply to Ne^{3+} , Ar^{3+} , Kr^{3+} , and Xe^{3+} .

Source	Uncertainty (in %)
Statistical uncertainty (typical value at peak cross section at 90% CL)	± 2
Form factor (total absolute uncertainty)	± 4
Additional systematic uncertainties:	
Particle-counting efficiency	± 3
Transmission to signal ion detector	± 4
Ion current	± 2
Electron current	± 2
Ion and electron velocities	± 1
Quadrature sum:	
Typical total uncertainty (good confidence)	± 7.4

two most interesting features of the measurements are the rise below the 60-eV threshold for ionization of the ground state ($3p^3^4S$) and the energy dependence at the maximum cross section, which is essentially constant from 100 to 240 eV. The rise below the ground-state threshold is due to metastables in the ion beam, as discussed in Sec. II A above.

A more subtle feature of the cross section is the rise from 57 to 70 eV which is faster than expected for direct ionization (for example, compare the experimental slope in this range to the slope of theories in the corresponding cross-section range). We suggest that this enhancement is due to indirect effects, such as excitation of an inner $3s$ electron to autoionizing states. This low energy excitation-autoionization enhancement could persist to quite high energies. In addition, the small feature beginning near 180-eV is attributed to excitation of inner $2p$ electrons followed by autoionization. This $2p$ - nl excitation may be to a number of final configurations (nl) and should have some of the same general character as the $2p$ - nl excitation autoionization which has been studied for Na-like ions.^{10,19} The net effect of the indirect processes for the Ar^{3+} case appears to be that the cross-section maximum is broader than expected from direct ionization alone.

Neither of the theories shown in Fig. 3 include metastable or indirect ionization contributions. Thus these theories might be expected to underestimate the measured cross section. Younger's DWX shows this expected comparison but the Lotz result, calculated from Eq. (1), is somewhat too high, particularly at high energies, as is often the case for light ions.⁴

Measurements of the electron-impact-ionization cross section for Ar^{3+} have previously been reported by Müller *et al.*¹¹ (open circles in Fig. 3, shown with 1 s.d. absolute uncertainties). The present results show good agreement with the previous measurements in cross-section shape, but the present results are up to 12% higher near the cross-section maximum, with better agreement at high and low energies. Even the 12% discrepancy is well within the combined absolute uncertainties of the experiments.

Figure 4 is a Bethe plot of the present data and theories. The influence of the ion-beam metastable content is clearly seen at low energies, where the experimental results appear high. This plot is particularly sensitive at high energies where any trends are magnified by the energy multiplication factor. The present data and Younger's DWX calculations are in good agreement over the entire energy range, and in particular, have the same slope at high energies. The Lotz calculations diverge, suggesting an overestimate of $2p^6$ direct ionization by the Lotz formula in this case.

C. Kr^{3+}

The ionization cross section versus electron energy for Kr^{3+} is shown in Fig. 5. Direct ionization of the ground state $4p^3^4S_{3/2}$ outer electron is expected at 50 eV, while ionization of the $4s$ and $3d$ inner-shell electrons begins at energies of 67 and 137 eV, respectively.

The experimental ionization onset is observed between 46 and 48 eV, indicating the presence of metastable ions. There is evidence for indirect effects close to the onset of ionization. The cross section rises more steeply than expected from threshold to about 80 eV, and then is essentially constant at a value of $35 \times 10^{-18} \text{ cm}^2$ to 115 eV. The steep rise and level behavior suggest a series of excitation-autoionization onsets. The decrease in cross section from 115 to 165 eV is more surprising than might appear at first glance, since the direct ionization cross section should be increasing in this energy range. Analysis of the cross section is complicated by uncertainty in the magnitude of the direct process, but the ionization fall-off with the Lotz contribution subtracted closely approximates an E^{-3} energy dependence (where E is the electron energy), characteristic of nondipole-allowed transitions.³³ One may speculate that the $3d$ electrons in Kr^{3+} are primarily responsible for unusual energy dependence observed in this cross section. Excitations of orbitals $3d$ - nl followed by autoionization could be responsible for most of the enhancement of the cross section over direct ionization. Excitation of $3d$ electrons contributing to photoionization of neutral Kr has been identified.^{34,35} However, an unusual enhancement observed in the direct photoionization of $3d$ electrons³⁵ is not apparent above the $3d$ direct ionization threshold in the present measurements.

Also shown in Fig. 5 are Lotz predictions for the direct ionization of Kr^{3+} . The Lotz predictions [from Eq. (1)] probably provide an upper limit for the direct ionization cross section. As has been noted, only half of the full d electron contribution to the cross section has been included in these calculations, but the Lotz predictions still overestimate the cross section by 67% at 1000 eV. It is obvious from Fig. 5 that the Lotz formula seriously underestimates the total ionization cross section at lower energies (less than 150 eV) due to neglect of indirect processes.

D. Xe^{3+}

The cross section for ionization of Xe^{3+} is shown in Fig. 6. Ionization from the $5p^3^4S_{3/2}$ ground state begins at 42 eV, with the $5s$ and $4d$ electrons ionizing at 53 and 104 eV, respectively.²⁸ Some metast-

able contribution at or below 37 eV is to be expected, as discussed in Sec. II A.

The arresting feature of the Xe^{3+} ionization cross section is of course the bump centered at 90 eV. This structure has the appearance of a resonance, but has a 60-eV FWHM and more than doubles the total cross section at its peak. At higher energies (above 200 eV) the cross-section shape and magnitude appear to be normal for direct ionization.

It appears that the Lotz cross section provides a good estimate of the direct ionization of Xe^{3+} , at least at medium and high energies (above 200 eV). As has been discussed, only half of the contributions of the d electrons has been included in the Lotz calculation. The inset in Fig. 6 shows the experimental data from 42 to 160 eV with the Lotz contribution (representing direct ionization) subtracted. This inset will be most useful in discussing the unusual effects observed in Xe^{3+} ionization.

There are fairly abrupt increases in the ionization cross section centered at 45, 64, and 71 eV with additional unresolved or smaller features at higher energies. The two lowest energy features (40–48 eV and 60–67 eV) are wider than our electron energy resolution, suggesting that more than single excitations are involved. In addition, attempts to calculate the energy levels of Xe^{3+} have not predicted autoionizing levels at such low energies.²⁸ The features centered at 45 and 64 eV may be due to recombination resonances which decay by double autoionization. Such recombination resonances would extend to energies below the corresponding excited states and could broaden the expected excitation features.^{13,14}

Recombination resonances might modify the low energy onset of excitation autoionization, but the bulk of the peak in the Xe^{3+} cross section must be due to excitations of the type $4d - nl$ which then autoionize. Numerous candidate excited levels lie in the region 70–90 eV.²⁸ However, the falloff of the cross section between 100 and 160 eV is surprising. The solid curve, in the inset of Fig. 6, has an energy dependence E^{-3} . This falloff suggests that the excitation autoionization proceeds dominantly through nondipole-allowed excitation transitions. Similar energy dependence is predicted³⁶ in the calculated indirect ionization cross section for Sb^{3+} .

A broad feature remarkably like the bump seen here was observed in photoionization of neutral Xe nearly 20 years ago,³⁷ and a few years later in photoabsorption.³⁴ This much-discussed “hump” was attributed to promotion of $4d$ electrons to continuum f levels³⁸ and occurred just above the $4d$ ionization threshold. Unusual effects and their causes have been discussed for various processes in neutral and ionized Xe,^{38–43} and similar effects have been ob-

served in neighboring elements.^{44–46} The feature observed in the photoionization of Xe and nearby atoms is due to unusually large direct ionization in the $4d - \epsilon f$ (continuum) channel.⁴⁶ A similar process in the present Xe^{3+} data would contribute at energies no lower than the 102-eV threshold for direct $4d$ ionization. In fact, the measured cross section is decreasing unusually fast in this energy range with no apparent features. Thus the overall bump in the Xe^{3+} data is believed to be due to excitation of $4d$ electrons followed by autoionization rather than unusual direct $4d$ ionization. In comparison, the photoionization of Ba and Ba^{2+} provides a similar trend,⁴⁵ since for Ba direct $4d$ photoionization produces a broad dominant feature while for Ba^{2+} , $4d - nf$ excitation followed by autoionization dominates. The general features of the Xe^{3+} ionization cross section, including the large bump, have also been observed in crossed electron-ion-beams experiments at Giessen⁴⁷ and additional experiments with other Xe ions are in progress in both laboratories.

E. Rates

Modeling the behavior of atomic species in a plasma requires a convolution of cross sections with a probability distribution over electron energies. It is generally assumed that the electron energies in a typical plasma can be represented by a Maxwellian distribution. To facilitate the utilization of the data presented here, Table III lists ionization rates for all four ions, corresponding to a convolution of the measured cross sections (extrapolated to higher energies than the experiments by scaling the Lotz predictions to match experiment at the highest energy measured) with a Maxwellian electron distribution. The computer code used for the convolution was developed at JILA⁴⁸ according to the formula

$$\langle \sigma v \rangle = \left[\frac{8}{\pi m_e} \right]^{1/2} (\alpha)^{1/2} \times \int_0^\infty \sigma(E) (E/\alpha) e^{-E/\alpha} d(E/\alpha), \quad (3)$$

where the rate $\langle \sigma v \rangle$ is expressed in units of cm^3/s , m_e is the electron mass, α is kT_e (where T_e is the electron temperature), and $\sigma(E)$ is the cross section at electron energy E .

The rates for ionization of Ne^{3+} , Ar^{3+} , Kr^{3+} , and Xe^{3+} are plotted in Fig. 7. Also plotted are the rate coefficients calculated using Lotz cross sections for the same species. Lotz rates may be approximated by a simple analytic formula to within a few percent.¹⁸ Because of the universality and simplicity of the Lotz rate formula, it is the most common source of rates for plasma modeling and analysis.

TABLE III. Experimental rates for triply charged inert gases (10^{-10} cm³/s).

Temperature (10 ⁶ K)	Equivalent energy (eV)	Ne ³⁺	Ar ³⁺	Kr ³⁺	Xe ³⁺
0.1	8.6			0.86	2.49
0.15	13.0		1.52	6.08	14.7
0.2	17.3		4.82	16.2	36.7
0.3	25.9	1.40	15.5	42.4	91.7
0.4	34.5	3.89	28.1	68.5	146.9
0.5	43.2	7.18	40.2	91.5	189.6
0.6	51.8	11.1	51.3	108.8	224.3
0.8	69.0	19.6	69.8	131.8	268.2
1.0	86.3	27.3	83.7	154.0	299.3
1.5	130.0	41.5	106.2	178.7	347.3
2.0	173.0	51.9	118.2	188.9	350.8
3.0	259.0	63.0	129.1	179.3	360.3
4.0	345.0	74.2	138.5	190.9	360.4
5.0	432.0	79.1	138.5	189.9	357.6
6.0	518.0	87.8	142.6	186.4	353.8
8.0	690.0	85.9	135.0	179.8	350.7
10.0	863.0	87.6	129.7	174.0	337.1
15.0	1295.0	88.2	126.7	162.5	318.9
20.0	1726.0	87.0	121.9	154.0	303.8
30.0	2589.0	83.7	114.3	141.8	280.7
40.0	3452.0	80.4	108.6	133.0	263.5
50.0	4315.0	77.4	104.0	126.2	250.0
60.0	5178.0	74.8	100.1	120.7	238.9
80.0	6904.0	70.5	94.0	112.1	221.7
100.0	8630.0	67.0	89.2	105.6	208.5
200.0	17260.0	56.2	74.6	86.6	170.1

Trends in the comparison of experimental and calculated rates in Fig. 7 can be predicted from the corresponding cross-section curves. For Ne³⁺, the rates from experiment and Lotz agree quite well at all temperatures, just as the cross sections agree. Ar³⁺ and Kr³⁺ Lotz calculations are too low at low

temperatures, and too high at temperatures above 0.7 and 1.5 million degrees, respectively. For Xe³⁺, substantial disagreement is seen at lower temperatures, but experiment and theory merge at higher temperatures. For the important low-temperature rise in the ionization rates, the experimental values exceed Lotz by more than a factor of 2 for Kr³⁺ and Xe³⁺.

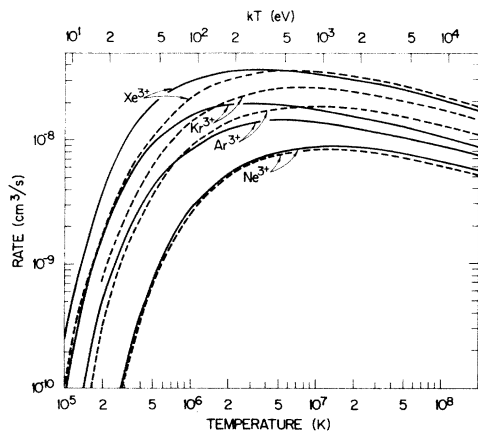


FIG. 7. Rate calculations from present data (solid curves) and Lotz rate calculations (dashed curves).

IV. CONCLUSIONS

On the simplest level, ionization of the four ions studied here might be expected to exhibit similar features. All four are triply charged inert-gas ions, with p^3 outer electron configurations, differing only in their inner-closed subshells. However, the features observed and the agreements with theory differ greatly in this series. The total ionization process becomes more complicated as the total number of electrons increase and the increasingly complicated inner-electron configurations make generalizations difficult.

The addition of d -shell electrons for the Kr³⁺ and Xe³⁺ cases appears to provide the most dramatic enhancements of the ionization cross sections.

Indeed *d*-shell electrons have provided a wealth of unexpected effects in similar studies of neutral atoms and singly charged ions. On the basis of previous studies, excitation autoionization could have been anticipated to enhance the cross sections for Ar^{3+} , Kr^{3+} , and Xe^{3+} , but the sharp falloff observed in both Kr^{3+} and Xe^{3+} was not expected. The unusual direct *4d* ionization process responsible for a large feature in the photoionization of neutral Xe is not responsible for the similar appearing feature in electron-impact ionization of Xe^{3+} since this direct feature would appear at significantly higher energy.

The Lotz formula provides a simple and reasonable estimate of direct electron-impact ionization. However, the present Ar^{3+} results illustrate that tractable quantum theory can provide more reliable results for direct ionization. The interpretation of the present Kr^{3+} and Xe^{3+} data could be improved if such theory were available for those cases. Nevertheless, the dominant problem illustrated by the present data is the indirect component (principally excitation autoionization) in complex ions. At present all theoretical estimates of electron-impact

ionization for complex ions (more than ten electrons) must be viewed as uncertain because of indirect effects and, based on the present results, the greater the electronic complexity the greater the uncertainty.

ACKNOWLEDGMENTS

The authors wish to thank J. W. Hale for technical assistance with the ion source and in daily operations. G. H. Dunn, R. A. Falk, and D. S. Belic from JILA participated in the assembly and alignment of the experimental apparatus. A number of theoreticians were helpful in interpreting the data, including D. C. Griffin, C. Bottcher, M. S. Pindzola, Y.-K. Kim, and S. M. Younger (who made his calculations available to us prior to publication). Finally, Val Kostroun first pointed out the resemblance of our data to photoionization measurements. This research was supported through the Office of Fusion energy of the U. S. Department of Energy under Contract No. W-7504-eng-26 with the Union Carbide Corporation.

-
- ¹See, for example, *Phys. Scr.* **23**, p. 69 (1981).
²D. E. Post, R. V. Jensen, C. B. Tarter, W. H. Grasberger, and W. A. Lokke, *At. Data Nucl. Data Tables* **20**, 397 (1977).
³W. Lotz, *Z. Phys.* **216**, 241 (1968).
⁴K. L. Bell, H. B. Gilbody, J. G. Hughes, A. E. Kingston, and F. J. Smith, Culham Laboratory Report No. CLM-R216, 1982, *J. Phys. Chem. Ref. Data* (in press).
⁵O. Bely, *J. Phys. B* **1**, 23 (1968).
⁶S. O. Martin, B. Peart, and K. T. Dolder, *J. Phys. B* **1**, 537 (1968).
⁷B. Peart and K. T. Dolder, *J. Phys. B* **1**, 872 (1968).
⁸D. H. Crandall, R. A. Phaneuf, and P. O. Taylor, *Phys. Rev. A* **18**, 1911 (1978).
⁹D. H. Crandall, R. A. Phaneuf, B. E. Hasselquist, and D. C. Gregory, *J. Phys. B* **12**, L249 (1979).
¹⁰D. H. Crandall, R. A. Phaneuf, R. A. Falk, D. S. Belic, and G. H. Dunn, *Phys. Rev. A* **25**, 143 (1982).
¹¹A. Müller, E. Salzborn, R. Frodl, R. Becker, H. Klein, and H. Winter, *J. Phys. B* **13**, 1877 (1980).
¹²R. A. Falk, G. H. Dunn, D. C. Griffin, C. Bottcher, D. C. Gregory, D. H. Crandall, and M. S. Pindzola, *Phys. Rev. Lett.* **47**, 494 (1981).
¹³K. J. LaGattuta and Y. Hahn, *Phys. Rev. A* **24**, 785 (1981).
¹⁴R. J. W. Henry and A. Z. Msezane, *Phys. Rev. A* **26**, 2545 (1982).
¹⁵R. D. Cowan and J. B. Mann, *Astrophys. J.* **232**, 940 (1979).
¹⁶D. H. Sampson and L. B. Golden, *J. Phys. B* **14**, 903 (1981).
¹⁷H. Jakubowicz and D. L. Moores, *J. Phys. B* **14**, 3733 (1981).
¹⁸D. H. Crandall, R. A. Phaneuf, and D. C. Gregory, Oak Ridge National Laboratory Report No. ORNL/TM-7020, 1979 (unpublished).
¹⁹D. C. Griffin, C. Bottcher, and M. S. Pindzola, *Phys. Rev. A* **25**, 154 (1982).
²⁰S. Suckewer, *Phys. Scr.* **23**, 72 (1981).
²¹S. M. Younger, *J. Quant. Spectrosc. Radiat.* **27**, 541 (1982); Ne^{3+} and Ar^{3+} results (private communication).
²²L. B. Golden and D. H. Sampson, *J. Phys. B* **13**, 2645 (1980).
²³W. T. Rogers, G. Stefani, R. Camilloni, G. H. Dunn, A. Z. Msezane, and R. J. W. Henry, *Phys. Rev. A* **25**, 737 (1982).
²⁴K. T. Dolder and B. Peart, *Rep. Prog. Phys.* **39**, 693 (1976).
²⁵P. O. Taylor, thesis, University of Colorado, 1972 (unpublished, available through University Microfilms, Ann Arbor, Michigan).
²⁶M. L. Mallory and D. H. Crandall, *IEEE Trans. Nucl. Sci.* **NS-23**, 1069 (1976).
²⁷S. Bashkin and J. O. Stoner, Jr., *Atomic Energy Levels and Grotrian Diagrams* (American Elsevier, New York, 1975), Vol. 1; Vol. 2 (1978).
²⁸D. C. Griffin (private communication). [The atomic structure and energies are calculated as described in D.

- C. Griffin, C. Bottcher, and M. S. Pindzola, *Phys. Rev. A* **25**, 1374 (1982).
- ²⁹P. O. Taylor, K. T. Dolder, W. E. Kauppila, and G. H. Dunn, *Rev. Sci. Instrum.* **45**, 538 (1974).
- ³⁰D. H. Crandall, J. A. Ray, and C. Cisneros, *Rev. Sci. Instrum.* **46**, 562 (1975).
- ³¹D. F. Dance, M. F. A. Harrison, and A. C. H. Smith, *Proc. R. Soc. London, Ser. A* **290**, 74 (1966).
- ³²M. F. A. Harrison, in *Methods of Experimental Physics* (Academic, New York, 1968), Vol. 74, pp. 95–115.
- ³³W. D. Robb, in *Atomic and Molecular Processes in Controlled Thermonuclear Fusion* (Plenum, New York, 1980), pp. 245–265.
- ³⁴R. Haensel, G. Keitel, P. Schreiber, and C. Kunz, *Phys. Rev.* **188**, 1375 (1969).
- ³⁵J. M. van der Wiel and G. R. Wight, *Phys. Lett.* **54A**, 83 (1975).
- ³⁶M. S. Pindzola, D. C. Griffin, and C. Bottcher, *Phys. Rev. A* (in press).
- ³⁷D. L. Ederer, *Phys. Rev. Lett.* **13**, 760 (1964).
- ³⁸J. W. Cooper, *Phys. Rev. Lett.* **13**, 762 (1964).
- ³⁹G. V. Gadiyak, D. A. Kirzhnits, and Yu. E. Lozovik, *Zh. Eksp. Teor. Fiz. Pis'ma Red.* **21**, 135 (1975) [*JETP Lett.* **21**, 6 (1975)].
- ⁴⁰M. Ya Amusia, V. K. Ivanov, and S. A. Sheinerman, *J. Phys. B* **9**, 1537 (1976).
- ⁴¹G. R. Wight and M. J. van der Wiel, *J. Phys. B* **10**, 601 (1977).
- ⁴²V. V. Afrosimov, Yu. S. Gordeev, V. M. Lavrov, and S. G. Shchemelinin, *Zh. Eksp. Teor. Fiz.* **55**, 1569 (1968) [*Sov. Phys.—JETP* **28**, 821 (1969)].
- ⁴³Z. Z. Latypov, S. E. Kupriyanov, and N. N. Tunitskii, *Zh. Eksp. Teor. Fiz.* **46**, 833 (1964) [*Sov. Phys.—JETP* **19**, 570 (1964)].
- ⁴⁴V. Pejcev, K. J. Ross, D. Rassi, and T. W. Ottley, *J. Phys. B* **10**, 459 (1977).
- ⁴⁵T. B. Lucatorto, T. J. McIlrath, J. Sugar, and S. M. Younger, *Phys. Rev. Lett.* **47**, 1124 (1981).
- ⁴⁶H. P. Kelly, S. L. Carter, and B. E. Norum, *Phys. Rev. A* **25**, 2052 (1982).
- ⁴⁷C. Achenbach, A. Müller, and E. Salzbom, Justus-Liebig Universität, Strahlenzentrum, Giessen, West Germany (private communication).
- ⁴⁸D. H. Crandall, G. H. Dunn, A. Gallagher, D. G. Hummer, C. V. Kunasz, D. Leep, and P. O. Taylor, *Astrophys. J.* **191**, 789 (1974).